L–H TRANSPORT BARRIER FORMATION: SELF-CONSISTENT SIMULATION AND COMPARISON WITH ASDEX U PGRADE EXPERIMENTS

T.P. KIVINIEMI, T. KURKI-SUONIO, S.K. SIPILÄ

Helsinki University of Technology, Department of Mathematics and Technical Physics, Euratom-TEKES Association, FIN-02015 HUT, Finland

J.A. HEIKKINEN

VTT Energy, Euratom-TEKES Association, P.O. Box 1604, FIN-02044 VTT, Finland

A.G. PEETERS

Max-Planck-Institut für Plasmaphysik - EURATOM Association, D-85748 Garching, Germany

Monte Carlo ion simulation based on neoclassical radial current balance near edge in a divertor tokamak geometry gives a stationary sheared $\vec{E} \times \vec{B}$ flow. The neoclassical radial electric field E_r shows no bifurcation in contrast with earlier orbit loss models, but the shear in E_r reaches values at which a transition to enhanced confinement has been observed. Also, MHD turbulence analysis shows that a smooth transition can occur through the neoclassical $\vec{E} \times \vec{B}$ flow shear suppression. The parameter scaling of threshold temperature for suppression of turbulence agrees with the H-mode threshold scaling in ASDEX Upgrade.

1 Introduction

Enhanced energy confinement is important in thermonuclear magnetic fusion since it can lead to an economically more attractive reactor. Experimentally, the anomalous transport has been found to decrease remarkably in the L–H transition, which, since its discovery in ASDEX tokamak in 1982 [1], has been observed in many divertor and limiter discharges, and also in some stellarators. Transition occurs when a threshold in the heating power is exceeded. In the L–H transition plasma jumps from the Low (L–) confinement mode into the High (H–) confinement mode, and the energy confinement time of the plasma is increased by a factor $f_H \approx 2$. This improvement in confinement is assumed to be due to sheared poloidal $\vec{E} \times \vec{B}$-rotation which builds up fast ($\approx 100\mu s$) in a narrow layer near the plasma edge during the transition. This rotation suppresses the turbulent fluctuations, and thereby the anomalous transport, by decorrelating neighboring eddies by the differential rotation [2]. Consequently, an edge transport barrier, with a width of 1-3 cm, is formed and fluctuations in magnetic field, density and electrostatic potential are reduced there. Particle diffusivity and heat conductivity are reduced by a factor of 5-10, which for ions means that, in this narrow layer, transport can be close to its neoclassical value. Although the rapid improvement in confinement has been known for long, the mechanism how the radial electric field is formed in the transition is still unclear. Spectroscopic measurements used for detecting E_r-profile do not have sufficient time resolution to decide the causality between the electric field and the improved confinement. The CX-signal,

observed by a neutral particle analyzer, gives a measure of E_r in the plasma periphery with much better time resolution but only a slow increase in E_r has been observed in those measurements so far [3].

At least three theories exist that can explain an L–H transition in agreement with the experimental observations. One candidate is the so-called 'Stringer spin-up' [4], in which a bifurcation in poloidal rotation occurs due to poloidally asymmetric particle source or transport. The second proposed explanation is based on an asymmetric fluctuation spectrum (Reynold's stress) [5] causing a flow generation. In both of these cases, the spin-up of the poloidal flow is assumed to occur due to anomalous processes. In the theory in Ref. [6], anomalous processes are not included, but the bifurcation is assumed to happen due to a multivalued balance between the ion orbit loss (OL) current and the neoclassical return current, when poloidal Mach number exceeds one.

In this paper, edge E_r profile from self-consistent, fully kinetic 5D neoclassical simulation of the tokamak edge with various plasma conditions is solved. Two different methods are used: Time dynamics of E_r are solved from the polarization equation or, alternatively, a steady-state E_r, which maintains a given density profile, is found by iteration. The orbit loss of both thermal and tail ions, the neoclassical ion return current, and the ion distribution asymmetrization by divertor losses and through redistribution by replacing ions (for charge neutrality) is included. For ASDEX Upgrade parameters no bifurcation in E_r is found, but the field changes smoothly, following the change in the plasma parameters. Although the poloidal Mach number can reach values larger than one, this occurs only in a region of a few mm, close to the separatrix, and is sensitive to changes in viscosity and the boundary conditions. The small radial extent of this region makes it unlikely that it plays an important role in the stabilization of turbulence. However, although the Mach number is smaller than one over most of the domain, it still has a high enough shear for turbulence suppression. This shear can appear within a wide enough radial region to a typical radial decorrelation length of the fluctuations.

Paper is organised as follows: The numerical methods, including the Monte Carlo code ASCOT and different methods for solving the radial electric field, are presented in Sec. 2. In Sec. 3, simulated E_r profiles are presented for different plasma parameters, classified according to their shear with respect to the BDT criterium, and the results are compared to the experimental scaling. In Sec. 4, the turbulence model and its results are presented. Finally, in Sec. 5, conclusions are given.

2 The numerical models

2.1 The Monte Carlo code ASCOT

In the 5D Monte Carlo code ASCOT [7], charged particle motion is followed in all three configuration space variables, but only in pitch and magnitude in velocity space, i.e., guiding centre approximation for the particle trajectories is used. Gyroangle dependence is not taken into account, because the time scale of the gyromotion is orders of magnitude faster, which would shrink the time step and, thus, increase the required CPU resources enormously. However, the effect of gyroviscosity is added using a simple analytic model. ASCOT is able to use

experimental background data as input. The collision operators are derived from the respective Fokker–Planck terms including slowing-down, energy diffusion and pitch angle scattering. The ion-electron collisions are now switched off, since we are not interested in ambipolar transport, which does not contribute to the current balance. The background density and temperature profiles are assumed to be due to anomalous effects due to their much larger transport fluxes. Anomalous fluxes are assumed to be ambipolar, i.e, they do not influence the current balance. Therefore, the requirement for zero steady-state radial current is dictated only by neoclassical effects. In modelling ion orbit loss current, neoclassical current and viscosity, the guiding centre equations of motion are solved for an ensemble of test ions, which are left to collide with a Maxwellian background distribution. As the background should rotate with the $\vec{E} \times \vec{B}$ -velocity, the influence of the electric field to the test particle velocity is omitted when evaluating the effect of collisions. A test particle in the simulation represents a group of particles initially distributed uniformly in configuration space and according to Maxwellian distribution in velocity space. Each test particle is weighted with a number that corresponds to the relative phase space volume of the initial position and velocity of the particle. Because the simulation of the whole plasma volume would require huge amounts of computer resources, and since only the edge region is interesting for our problem, it is well justified to limit the simulation only to a small radial region near the separatrix. In order to avoid losing particles from the simulation regime, inside the inner simulation boundary we switch off the collisions and evaluate the unperturbed particle trajectories as shown in Fig. 1. Since in the code the density is calculated from the accumulative time the particles spend in each cell, the particle time is not advanced while the particle is outside the simulation regime, i.e., every particle that crosses the inner boundary flux surface comes back to the simulation regime instantaneously.

The particle is lost if it intersects the divertor plate or wall structure. These particles are promptly reinitialized back to the plasma at the separatrix with local thermal velocity and uniformly in pitch and poloidal angle in order simulate the replacement of lost charge through separatrix which is much more uniform in phase space than the loss process. The reinitialization is done at the separatrix, because it is important not to introduce any unphysical currents which could influence the balance between the neoclassical return current and the ion orbit loss current. Outside the separatrix the electric field cannot be determined. Similarly to the inner boundary, also at the separatrix the accumulation of particle time is stopped when the particle leaves the simulation regime until it comes back, or until it is lost and reinitialized back to the simulation regime. However, here we do not turn off the collisions outside the simulation regime but the particle is allowed to collide with the background plasma outside the separatrix.

2.2 Solving E_r from polarization equation

In the code, the ion ensemble corresponding to the main plasma ions is initially distributed according to the assumed background density and temperature with Maxwellian energy distribution. Each ion is followed along its guiding centre orbit determined by the $\vec{E} \times \vec{B}$-, gradient- and curvature-drifts, collisions as well as polarization- and viscosity-drifts. The radial electric field E_r on a magnetic surface with coordinate ρ is evaluated from [8]

$$\partial E_r/\partial t = -(\Omega B_t/n)\Gamma_{NC}, \tag{1}$$

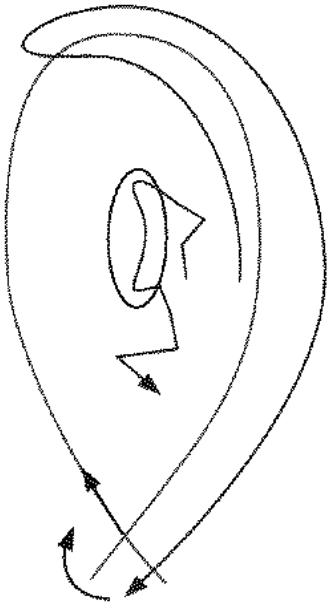

Fig. 1. If the inner boundary is crossed, the particle trajectory is followed in the absence of collisions until it comes back to the simulation regime. Outside the separatrix collisions are present. Lost particles are reinitialized to the separatrix, with thermal velocity and randomly distributed in pitch and poloidal angle.

where n is the density, B_t is toroidal magnetic field, $\Omega = e_i B/m_i$ with test particle mass m_i and charge e_i, and Γ_{NC} is the particle flux at the radius ρ as calculated from ion motion excluding the flux due to polarization drift. Therefore, $\Gamma_{NC} = \Gamma_{tot} - \Gamma_{pol}$, where

$$\Gamma_{pol} = (n/\Omega B_t)\partial E_r/\partial t \tag{2}$$

is the polarization drift and Γ_{tot} is the total radial velocity of the ensemble at ρ. From Eqs. (1) and (2) it follows that $\Gamma_{tot} = 0$ which, in fact, is the condition $j_r = 0$ for current density. Thus, the density profile $\langle n(\rho, \theta)\rangle$, where θ is the poloidal angle, is automatically kept constant. Formally, the radial flux Γ_{NC} can be written as

$$\Gamma_{NC} = \Gamma_{coll} + \Gamma_{loss} + \Gamma_{gyro}, \tag{3}$$

in which the last term is included using an analytic theory [9] where the radial drift due to gyroviscosity is estimated to be

$$\Gamma_{gyro} = -\frac{\eta}{e_i B^2}\frac{\partial^2 E_r}{\partial r^2}, \tag{4}$$

with the Braginskii viscosity coefficient $\eta = (3/10)nT(\nu_{ii}/\Omega^2)$ with temperature T and ion-ion collision frequency ν_{ii}. This is explicitly added to the particle motion, as it has importance especially in high shear regions. Since gyroviscosity is a contribution of the form $\partial_t E_r = f\partial_{rr}E_r$ where $f = f(n, T, B_t, ...)$, the timestep τ and the other simulation parameters have to fulfil the Courant condition, $\tau \leq (\Delta r)^2/2f$, in order to obtain stable solutions.

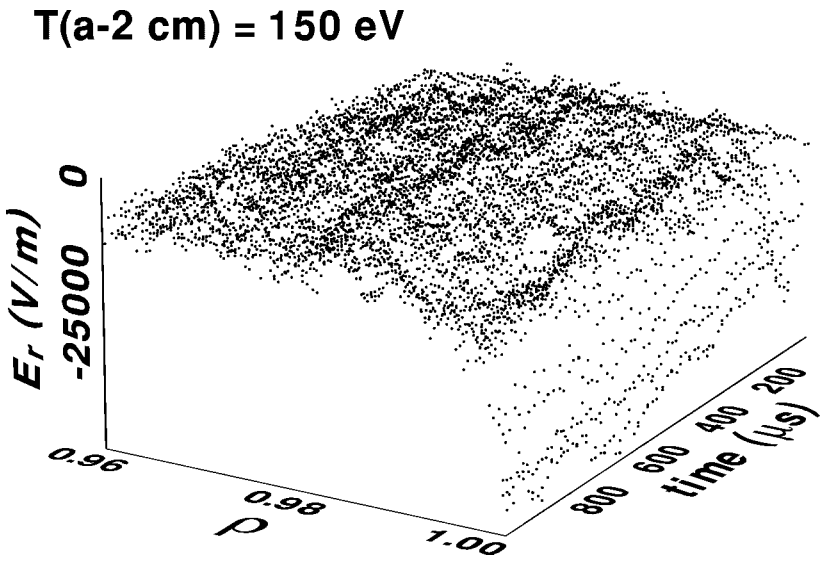

Fig. 2. Radial electric field profile as a function of time as calculated from Eq. (1).

An example of the time dynamics of the electric field radial profile is shown in Fig. 2. Because initialization is only an approximation of the distribution of the particles in phase space, it is important to do the simulations in a collisional time scale so that the effect of the initialization will be erased and steady-state is reached.

2.3 Iterating for E_r in a realistic geometry

Here, an alternative method to solve E_r is introduced. We do not follow the evolution of the electric field in time, but rather try to find the steady-state value. Our aim is to iterate the self-consistent electric field that maintains the test particle density profile consistent with the background density profile and, thus, gives zero radial ion flux. The self-consistent steady-state radial electric field is here defined as the field for which the following two requirements are fulfilled:

1. the density profile is stationary

2. the test particle density profile remains consistent with the background

In standard neoclassical theory a change in the gradient of the density profile corresponds to a change in the electric field because, in steady-state, the flux Γ is zero. However, updating the electric field by calculating the derivative of the test particle density profile and comparing it to the background density profile would cause large errors, because the stochastic noise would have a great effect in calculating the derivatives. Also, the requirement of the vanishing flux alone is not enough to get the correct electric field since the test particle distribution changes in the beginning of the iteration, and we most probably would find the balance for a wrong density profile. To avoid this, we reformulate our second requirement in a following way: Beginning from the background density profile, the test particle density profile after time t is consistent with the background if

$$\int_0^t \Gamma(r)dt = 0, \tag{5}$$

for which, using the continuity equation,

$$\frac{\partial n}{\partial t} + \nabla \cdot \Gamma = 0 \tag{6}$$

we get the expression

$$\int_0^t r\Gamma(r)dt = -\int_r^a rn(r,t)dr + C, \tag{7}$$

where n is the test particle density, the integration constant is $C = \int_c^a rn_{bg}(r)dr$, n_{bg} is the background density and c is the inner edge of the simulation region. Typically the simulation regime spans only a few centimeters, i.e., only the regime where the ion orbit losses are likely. The test particle density is calculated as a time average over the iteration time step τ_{it}. Based on Eqs. (1) and (7), the following method has been found successful in a non-circular geometry: After time τ_{it}, the radial electric field at location ρ is updated to the value $E_r^* = E_r + dE_r$ with

$$dE_r(\rho,t) = \alpha \int_\rho^{\rho_{sep}} [n(\rho,t) - n_{bg}(\rho)]dV, \tag{8}$$

where the upper boundary ρ_{sep} is at the separatrix, dV is the volume element, and α is an iteration parameter depending on τ_{it} and plasma parameters. In order to avoid fluctuations, the update in Eq. (8) is done only if the difference in test particle and background density profiles is increasing in time. If the test particle density profile is close enough to the background density profile after k iterations, only a slight change in E_r due to stochastic oscillations in density can be observed, and the obtained E_r is considered to be self-consistent.

Unlike in the previous section, when iterating for the steady-state E_r-profile, the polarization drift is neglected, and we assume that Γ is purely caused by the neoclassical flux due to Coulomb collisions. Leaving out the polarization drift allows us to use a relatively small number of test particles and a large iteration time step. In order to avoid the effect of an unphysical initialization in the results, simulation time has to span collisional time scale $\tau_{coll} \sim 1/\nu_{ii}$ as in the previous section.

As an example of an iteration of the electric field, starting at the ambipolar value using ASDEX Upgrade data is shown in Fig. 3. Although the iteration shows similar charateristics as in Fig. 2 where E_r is solved from polarization equation, evolution of E_r is here purely numerical, i.e., only the steady-state has a physical meaning. Both the solving the evolution of E_r from polarization equation and the iteration method presented here have resulted with the same steady-state.

3 Results

In this section we study the dependence of E_r on temperature and density profiles. We first look at the region $\rho \geq 0.99$, where the E_r-gradient in the absence of gyroviscosity is very steep due to strong effect of ion orbit losses. Later, gyroviscosity is included, and we assume that the relevant region for confinement improvement is broader and the gradient of E_r further inside, although it is much more gently sloping, may still be sufficient to fulfil the BDT criterium. As the criterium requires strong enough shear at least in a 0.7 cm wide region inside the separatrix, we simulate a 2 cm wide regime.

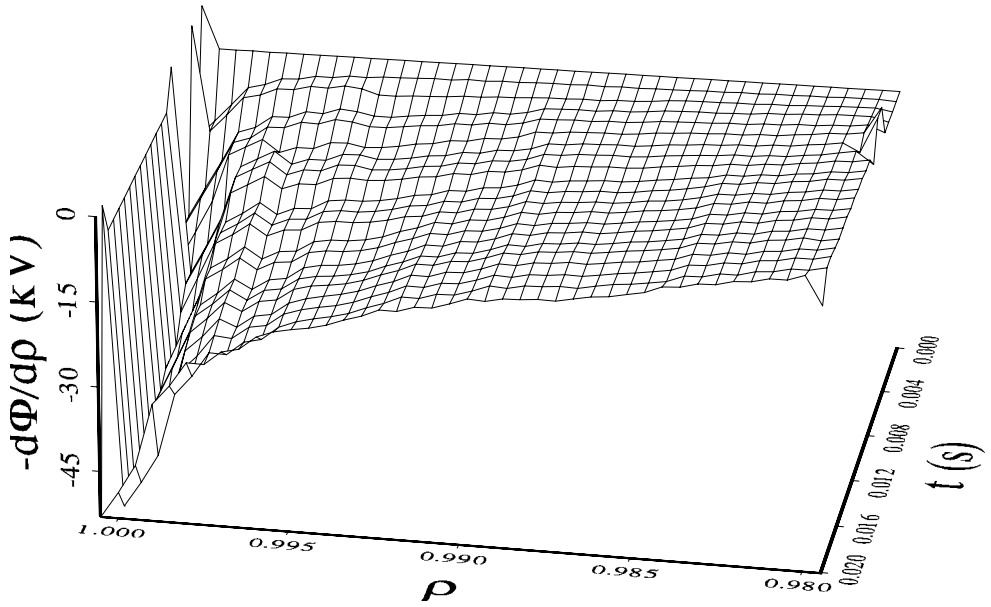

Fig. 3. Convergence of the electric field during an iteration.

3.1 Steady-state profiles

In the simulations, ASDEX Upgrade configuration and parameters are used. The minor radius is $a = 0.5$ m, major radius $R = 1.65$ m, elongation 1.6, plasma current $I = 1$ MA, and $B_t = -2.5$ T. Corresponding to the shot #8044 for a deuterium plasma, a separatrix density 1.2×10^{19} m^{-3} and temperature 120 eV with about 1.9 times larger values at $r = a - 2$ cm are adopted as a reference case.

In order to compare our results to the OL theory in Ref. [6] we first leave out the gyroviscosity. We express E_r in terms of poloidal Mach number because, according to the theory, bifurcation occurs when M_p exceeds unity due to decreasing collisionality. In Fig. 4, the collisionality is varied by scaling the temperature and density profiles by constant factors. The electric field profiles of are plotted in terms of $M_p^* = (E_r - E_{ambi})/v_{ti}B_p$. The electric fields E_r and E_{ambi} are defined at the outboard equator. Contribution of the ambipolar electric field is substracted in order to see how much E_r deviates from its ambipolar value. In contradiction to OL theory, the magnitude of E_r and, thus, $|M_p^*|$ reduces if the collisionality is decreased by scaling the density. Also, changing the collisionality by scaling the temperature shows the desired ν_{*i}-dependence only within a region which is less than 1 mm within the separatrix.

It is clear that, without gyroviscosity, the monotonically (in radius) increasing ion orbit loss would cause monotonically increasing negative electric field towards the separatrix, which is inconsistent with the experiments, where the field outside the separatrix is positive and has a positive gradient. For this reason it is important to take into account classical effects. In the simulations, electrons are not included. Outside the separatrix, the rapid motion of the electrons along the field lines guarantees that, at all surfaces, the electrostatic potential stays close to that of the divertor plates. This deficiency in the model can be eliminated by imposing a positive or zero electric field outside the separatrix, and by including the effect of viscosity. Viscosity couples the rotation speeds at neighbouring magnetic surfaces inside the separatrix, causing E_r to bend towards the imposed zero electric field at the edge.

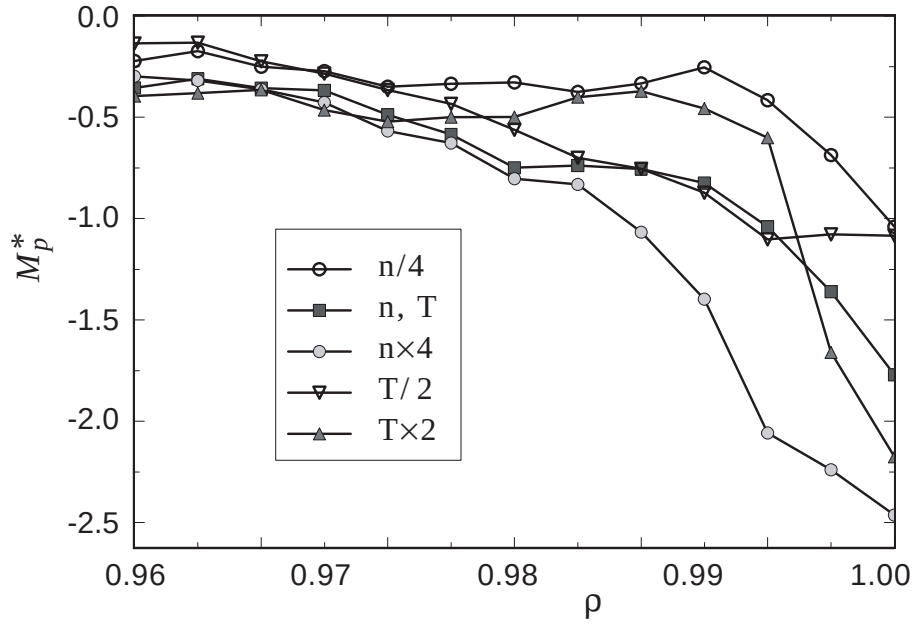

Fig. 4. $M_p^* = (E_r - E_{ambi})/v_{ti}B_p$ values for the iterated E_r profiles. Inside the plasma E_r is close to E_{ambi}, i.e. $|M_p^*| \ll 1$, but near the edge where the ion orbit losses have strong effect, $|M_p^*|$ can exceed one.

Fig. 5 shows the steady-state profiles of $-d\Phi/d\rho$ in the region $0.96 < \rho < 1$ ($\rho_{sep} = 1$) for different temperature profiles which are obtained by scaling the reference profile. The numerical value for E_r at the outboard equator is found by multiplication by the geometric factor $d\rho/dr = 2$ m^{-1} The higher the temperature, the steeper the gradient of E_r. In the simulation, the dependence of the gradient of E_r on density, plasma current and toroidal magnetic field was found to be weak. The best fit for the shear in the numerical (deuterium) data is given by $\langle dE_r/dr\rangle/B = 2964 \cdot T^{1.06} n^{0.06} B_t^{-0.81} I^{-0.27}$ s^{-1} with ± 0.25 error in exponents.

3.2 Scaling of the critical edge temperature

The experimental scaling for the critical edge electron temperature at ASDEX Upgrade is [10]

$$T_e(a - 2\mathrm{cm}) = 145 \left(\frac{n}{10^{19}\mathrm{m}^{-3}}\right)^{-0.3} \left(\frac{B_t}{1\mathrm{T}}\right)^{0.8} \left(\frac{I_{pl}}{1\mathrm{MA}}\right)^{0.5} \mathrm{eV}, \tag{9}$$

which shows the relevant variables for the L–H transition. In order to compare our simulation results to the experiments, the iterated E_r-profiles are here classified using the BDT criterium [2] for the suppression of turbulence. The criterium is based on the assumption that the turbulent fluctuations consist of eddies of radial extent Δr_t, with a typical lifetime τ_{eddy}, and a poloidal extent $1/k_\theta$, where k_θ is a typical poloidal wavenumber for the fluctuations. From the radial derivative of the $\vec{E} \times \vec{B}$ -velocity, one can calculate the time it takes to tear apart neighbouring eddies. Comparing this to a typical eddy lifetime leads to the criterium

$$\left|\frac{dE_r/dr}{B}\right| > L_{shear} \sim 10^5 - 10^6 s^{-1}, \tag{10}$$

in which $L_{shear} = (\Delta r_t k_\theta \tau_{eddy})^{-1}$. If this condition holds for at least a 0.7 cm-wide regime inside the separatrix, the shear can be considered to be strong enough to suppress the transport.

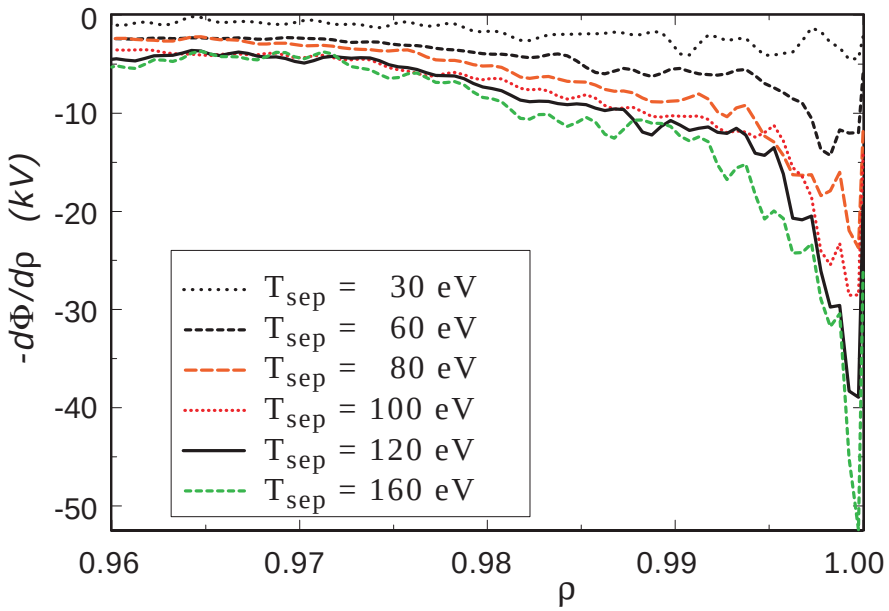

Fig. 5. Iterated electric fields for different temperatures.

Otherwise, the shear is assumed to be too low, corresponding to L–mode. For the limit, we choose a value $L_{shear} = 5 \times 10^5$ s^{-1}. In Fig. 6, the electric field profiles of all simulation are classified using the criterium. To ease the comparison with experiments, the simulation temperature is plotted as a function of the experimental scaling of Eq. 9. The experimental scaling is plotted with a dashed line. Comparing the numerical simulations and the experimental results, a good agreement is found. By introducing $L_{shear} = 5 \times 10^5$ s^{-1} into the numerical fit of the shear in the previous section, one obtains for the critical temperature $T_{cr} = 126 n^{-0.06} |B_t|^{0.76} I^{0.25}$ eV. The parameters were varied in the range $B_t = -1.1 - (-5.0)$ T, $I = 0.6 - 1.5$ MA, $n = 0.6 - 9 \times 10^{19}$ m^{-3}, and $T = 30 - 400$ eV, broader than in the experiments. Shear dependence on n and T was found to be stronger in the lower n and T data range, respectively. However, the number of data points in Fig. 6 is small and there is some freedom in choosing the values for the BDT criterium.

4 Turbulence

To show that the sheared flow generated by orbit loss can significantly suppress turbulence near T_{cr} in Fig. 7, MHD turbulence with the simulated $\vec{E} \times \vec{B}$ flow shear was resolved. As a paradigm for self-organized tokamak plasma edge turbulence, resistive drift wave equations [11] for the nonlinearly unstable vorticity, density, temperature, and parallel electron velocity fluctuations were adopted, and they were complemented with the equation

$$\partial v_E / \partial t = \sum_{m=-M}^{M} imk_0 (\Phi_{-m} \partial^2 \Phi_m / \partial x^2) / B_0^2 + \nu [v(x,t) - v_E] \qquad (11)$$

describing the evolution of the average poloidal $\vec{E} \times \vec{B}$ flow velocity $v_E = \hat{z} \times \nabla \Phi_0 / B_0 = (\partial \Phi_0 / \partial x) \hat{y} / B_0$ in the presence of the electrostatic potential $\Phi = \sum_{m=-M}^{M} \Phi_m(x) \exp(imk_0 y)$ and orbit loss driven poloidal $\vec{E} \times \vec{B}$ flow $v(x,t)$. Here, a sheared two-dimensional slab with

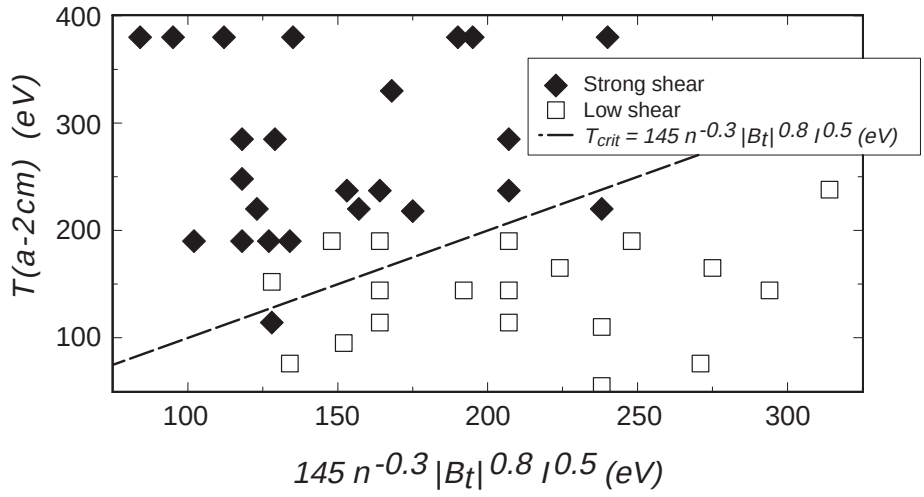

Fig. 6. Classified $\vec{E} \times \vec{B}$ velocity shear from ASCOT simulations. If condition $|dE_r/dr|/B > 5 \times 10^5$ s^{-1} holds within 0.7 cm inside the separatrix, the shear is here considered to be strong, otherwise low. The results agree well with the experimental scaling (dashed line).

x and y corresponding to the radial and poloidal directions, respectively, was adopted with $L_y = 2\pi/k_0$ and $2L_x$ the lengths of the slab in the y and x directions, respectively. The first term on the right hand side in Eq. (11) is the turbulent Reynolds stress, and the second term with $\nu = qv_T/R$ models the viscosity. Single-helicity turbulence resonant at $x = 0$, and local magnetic shear $B = B_0(1 + x/L_s)$ with background gradients $dn/dx = -n_0/L_n$ and $dT/dx = -T_0/L_T$ were considered. Using our reference parameters, and $T_0 = 100$ eV, $n_0 = 4 \times 10^{19}$ m^{-3}, $L_n = L_T = 0.02$ m, $L_s = 2$ m, $L_y = 0.02 \times \pi$ m, and $L_x = 0.015$ m, turbulence was followed for various values of shear, $V' = dv/dx$, at $x = 0$ with nonlinearly unstable initial amplitudes of Φ_m. Fig. 7 shows the evolution of the kinetic energy $E_k = m \int_A |\nabla\hat{\Phi}/B_0|^2 da/2L_y$ in units of $mk_0^{-2}\omega_\star^2 r_L/2$ for $V' = 0, 3, 6,$ and 9×10^5 s^{-1}. Here, $\omega_\star = k_0 T_0/eB_0L_n$ is the drift wave angular frequency, r_L is the ion Larmor radius, $\hat{\Phi} = \Phi - \Phi_0$, and $\int_A$ denotes surface integral over the slab. In simulations, $2M + 1 = 121$ modes with 151 grid points in x were used. A nonlinearly saturated turbulence with a strongly suppressed level for largest V' is found. Suppression grows gradually with V' and becomes significant for $V' \sim 5 \times 10^5$ s^{-1}. Quantitatively similar results were also found for the pressure-gradient driven turbulence, which was resolved using a model similar to that in Ref. [12]. Turbulence suppression and perturbations in v_E by the Reynolds stress were weak and always dominated by the orbit loss driven flow near the threshold conditions in Fig. 7. The results thus support the picture of Fig. 7 that the orbit loss driven shear suppresses the turbulence, and that this effect becomes pronounced around the transition threshold. The results also support the measurements in reversed field pinch configurations, where a naturally occuring double velocity shear layer has been identified at the edge with a shear value comparable to that in tokamaks and stellarators, and most probably originating from finite Larmor radius losses [13].

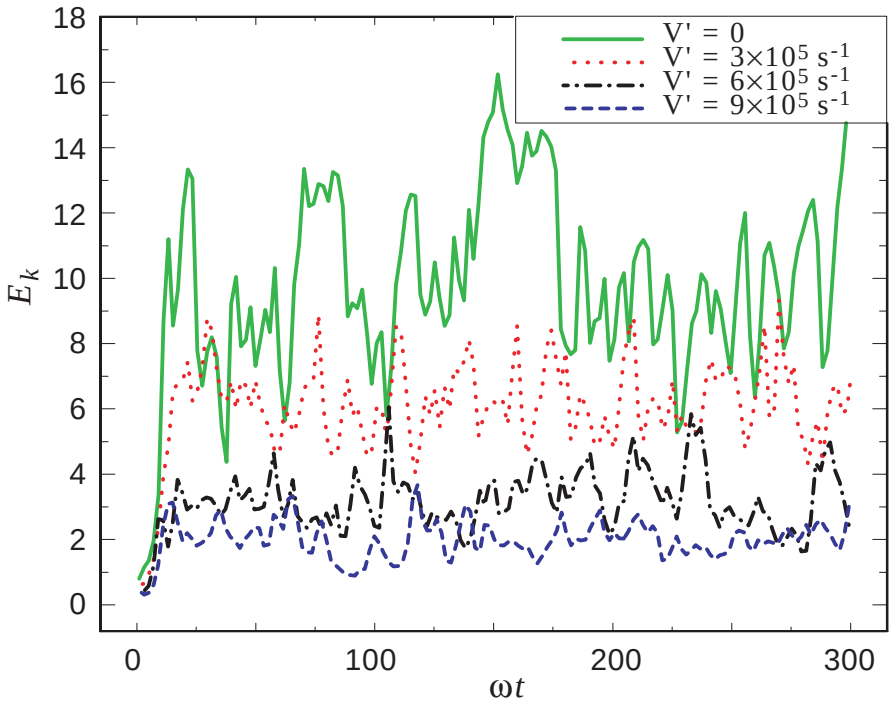

Fig. 7. Kinetic energy E_k in potential fluctuations (in arbitrary units) with various shears V'.

5 Conclusions

The main result of this study is that, although we did not see a bifurcation, the gradient of E_r for typical H–mode parameters at the edge can be large enough to suppress turbulent fluctuations there. When compared to the experimental scaling for the H–mode threshold, numerical simulations show similar characteristics, when BDT criterium was used to classify the E_r-profiles according to the magnitude of their shear. The present simulations do not explain the reason for the L–H transition, but it was shown that, in H–mode conditions, the radial electric field due to purely neoclassical effects is sufficient to suppress anomalous transport. If the edge ion temperature grows slowly during external heating, only a slow transition can appear, if the shear reduces transport smoothly as in the MHD turbulence simulation presented here. Some tokamak experiments [14, 15] see a neoclassical ambipolar E_r just before the transition, and a fast suppression of turbulence at the transition on a time scale much shorter than changes in background temperature. In order to reconcile the present findings with them, a mechanism which can restrain OL driven rotation in L-mode and allow it in H-mode is required.

This work benefited from the computing resources of the Centre of Scientific Computing in Espoo, Finland.

References

[1] F. Wagner *et al.*: Phys. Rev. Lett. **49** 1408 (1982).

[2] H. Biglari, P.H. Diamond, P.W. Terry: Phys. Fluids B **2** (1990) 1.

[3] W. Herrmann *et al.*: Phys. Rev. Lett. **75** (1995) 4401.

[4] A.B. Hassam, T.M. Antonsen, Jr., J.F. Drake, and C.S. Liu: Phys. Rev. Lett. **66** (1991) 309.

[5] P.H. Diamond, Y.-B. Kim: Phys. Fluids B **3** (1991) 1626.

[6] K.C. Shaing and E.C. Crume, Jr.: Phys. Rev. Lett. **63**, (1989) 2369.

[7] Seppo Sipilä: *Dissertation*, Helsinki University of Technology, Espoo (1997), ISBN 951-22-3856-X, http://www.hut.fi/Units/AES/ascot.html;
J.A. Heikkinen, S.K. Sipilä: Phys. Plasmas **2** (1995) 3724.

[8] S.V. Novakovskii, C.S. Liu, R. Sagdeev, and M.N. Rosenbluth: Phys. Plasmas **4** (1997) 4272.

[9] L. Spitzer, Jr.: *Physics of Fully Ionized Gases.* 2nd Edition, Interscience Publishers (a division of John Wiley & Sons), New York, 1962.

[10] W. Suttrop *et al.*: Plasma Phys. Contr. Fus. **39** (1997) 2051.

[11] B.D. Scott: Phys. Fluids **B4** (1992) 2468.

[12] H. Sugama and W. Horton: Phys. Plasmas **1** (1994) 345.

[13] V. Antoni *et al.*: Phys. Rev. Lett. **79** (1997) 4814.

[14] P. Gohil, K.H. Burrell, and T.N. Carlstrom: Nuclear Fusion **38** (1998) 93.

[15] R.A. Moyer *et al.*: Phys. Plasmas **2** (1995) 2397.